REPORT DOCUMENTATION PAGE

1. REPORT DATE (DD-MM-YYYY)
05-10-2005

2. REPORT TYPE
REPRINT

4. TITLE AND SUBTITLE
Fast coronal mass ejection environments and the production Of solar energetic particle events

5a. CONTRACT NUMBER

5b. GRANT NUMBER

5c. PROGRAM ELEMENT NUMBER
61102F

6. AUTHOR(S)
Kahler, S.W. and A. Vourlidas*

5d. PROJECT NUMBER
2311

5e. TASK NUMBER
RD

5f. WORK UNIT NUMBER
A1

7. PERFORMING ORGANIZATION NAME(S) AND ADDRESS(ES)
Air Force Research Laboratory/VSBXS
29 Randolph Road
Hanscom AFB MA 01731-3010

8. PERFORMING ORGANIZATION REPORT NUMBER

AFRL-VS-HA-TR-2007-1046

9. SPONSORING / MONITORING AGENCY NAME(S) AND ADDRESS(ES)

10. SPONSOR/MONITOR'S ACRONYM(S)
AFRL/VSBXS

11. SPONSOR/MONITOR'S REPORT NUMBER(S)

12. DISTRIBUTION / AVAILABILITY STATEMENT
Approved for Public Release; Distribution Unlimited.

*NRL, Washington, DC

14. ABSTRACT The search continues for coronal environmental factors that determine whether a fast coronal mass ejection (CME) results in a solar energetic particle (SEP) event at 1 AU. From a plot of peak 20 MeV SEP intensities versus associated CME speeds we select for comparison two groups of fast, wide, western hemisphere CMEs observed with the LASCO coronograph from 1998 to 2002. The SEP-rich CME group produced the largest observed SEP events, and the SEP-poor CME group produced the smallest or no observed SEP events. The major differences are that the SEP-rich CMEs are brighter and more likely to be streamer blowouts and to follow colocated CMEs within 12 or 24 hours. The SEP-poor CMEs are fainter and less likely to interact with streamers or to follow preceding colocated CMEs. Thus we confirm the recent result that the SEP event peak intensities are higher when the associated driver CMEs are preceded within a day by wide CMEs at the same locations. However, the enhanced brightness, and therefore mass, of the SEP-rich CMEs appears to be their most dominant characteristic and suggests that either large longitudinal and latitudinal extents or higher densities are needed for fast CMEs to produce SEPs.

15. SUBJECT TERMS
Sun, Corona, Coronal mass ejections, Particle emission

16. SECURITY CLASSIFICATION OF:

a. REPORT	b. ABSTRACT	c. THIS PAGE
UNCLAS	UNCLAS	UNCLAS

17. LIMITATION OF ABSTRACT
SAR

18. NUMBER OF PAGES
10

19a. NAME OF RESPONSIBLE PERSON
S. W. Kahler

19b. TELEPHONE NUMBER (include area code)
781-377-9665

Fast coronal mass ejection environments and the production of solar energetic particle events

S. W. Kahler

Space Vehicles Directorate, Air Force Research Laboratory, Hanscom Air Force Base, Massachusetts, USA

A. Vourlidas

Code 7663, Naval Research Laboratory, Washington, DC, USA

[1]   The search continues for coronal environmental factors that determine whether a fast coronal mass ejection (CME) results in a solar energetic particle (SEP) event at 1 AU. From a plot of peak 20 MeV SEP intensities versus associated CME speeds we select for comparison two groups of fast, wide, western hemisphere CMEs observed with the LASCO coronagraph from 1998 to 2002. The SEP-rich CME group produced the largest observed SEP events, and the SEP-poor CME group produced the smallest or no observed SEP events. The major differences are that the SEP-rich CMEs are brighter and more likely to be streamer blowouts and to follow colocated CMEs within 12 or 24 hours. The SEP-poor CMEs are fainter and less likely to interact with streamers or to follow preceding colocated CMEs. Thus we confirm the recent result that the SEP event peak intensities are higher when the associated driver CMEs are preceded within a day by wide CMEs at the same locations. However, the enhanced brightness, and therefore mass, of the SEP-rich CMEs appears to be their most dominant characteristic and suggests that either large longitudinal and latitudinal extents or high densities are needed for fast CMEs to produce SEPs.

1. Introduction

[2]   There is substantial evidence that gradual solar energetic particle (SEP) events observed at 1 AU result from acceleration at coronal and interplanetary shocks driven by fast coronal mass ejections (CMEs) [Reames, 1999; Kahler, 2001]. CME speeds have been found to correlate with the peak intensities of the associated SEP events, but a very broad scatter in that correlation indicates a complexity in the shock acceleration process that is not understood.

[3]   Recent work has begun to explore the effects that variations in the coronal magnetic and particle environment might have in the resulting SEP production by CME-driven shocks. Enhanced decametric-hectometric (DH) emission was observed during interactions of a fast CME with a preceding slower CME on 10 June 2000 [Gopalswamy et al., 2001b] and on 3 September 1999 [Gopalswamy et al., 2002a] in the 5 to 10 $R_\odot$ height range. The enhanced DH emission was interpreted as evidence for the strengthening of a preexisting shock in the first case and for the formation of a new shock in the second [Gopalswamy et al., 2002a].

[4]   The possibility that interacting CMEs are important for ion acceleration in CME-driven shocks was explored by Gopalswamy et al. [2002b], who studied CMEs associated with $E > 10$ MeV SEP events with peak intensities ≥ 1 particle cm^{-2} s^{-1} sr^{-1} (pfu). They found that the great majority (68 of 81) of SEP-associated CMEs interacted with preceding CMEs within 50 $R_\odot$, as indicated by observed spatial overlap between the preceding and primary CMEs. In their inverse study of 52 fast (>900 km s^{-1}) and wide (>60°) frontside, western hemisphere CMEs, 10 were not associated with SEP events, but six of those 10 nevertheless interacted with preceding CMEs. A subsequent study [Gopalswamy et al., 2003a] found that five of those six preceding CMEs were very narrow, suggesting weak CME interactions as the reason for the lack of SEP production in those cases. In addition, seven of the 42 CMEs with SEP events did not interact with preceding CMEs, but in four of those seven cases the primary CMEs, all associated with major SEP events, interacted with and completely destroyed dense streamers. The basic interpretation [Gopalswamy et al., 2003a] of these results was that the efficiency of particle acceleration is somehow enhanced when the primary CME runs into regions of enhanced density due to preceding CMEs or to streamers.

[5]   The conclusion that a major fraction of SEP events occur at times of CME interaction [Gopalswamy et al., 2002b] was criticized by Richardson et al. [2003] on the basis that SEP production begins well before the CME interactions; the results were consistent with chance associations between preceding and primary CMEs; and the majority of preceding CMEs either faded into the back-
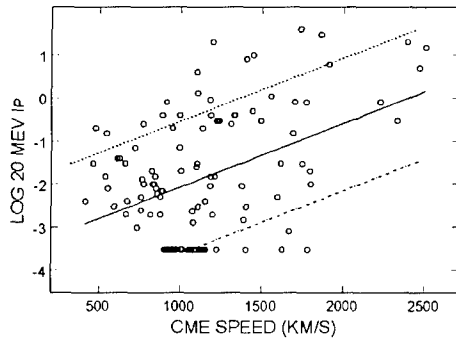
Figure 1. Plot of logs of Energetic Particles: Acceleration, Composition, and Transport (EPACT) instrument 20 MeV proton peak intensities versus the associated LASCO coronal mass ejection (CME) speeds for 116 wide CMEs in the W30° to >WL longitude range. The solid line is the least-squares best fit to the data. The solar energetic particle (SEP)-rich CMEs are the data points above the dashed line, and the SEP-poor CMEs are those below the dashed-dotted line. The two groups are separated by three orders of magnitude in SEP peak intensities. The cluster of points at ~1000 km s^{-1} are CMEs above the 900 km s^{-1} fast-speed threshold with no associated SEP events.

ground or were narrow, suggesting weak interactions between the CMEs. *Kahler* [2003] also argued that shock SEP acceleration would be diminished in the region of the preceding CME and that the magnetically closed field topology of the preceding CME would inhibit SEP escape from the shock region [*Vandas and Odstrcil*, 2004].

[6] These critiques, however, do not rule out a role for preceding CMEs or streamers as significant environmental factors [*Gopalswamy et al.*, 2003a] in the production of SEP events at CME-driven shocks. Recently, *Gopalswamy et al.* [2003b, 2004] changed their approach from the previous concept of leading-edge interaction between the preceding and primary CMEs to one of CME environmental preconditioning. They selected CMEs associated with large (>10 pfu) E > 10 MeV SEP events and searched for all wide (>60°) CMEs over the preceding 24 hours from the same source regions as the primary CMEs. *Gopalswamy et al.* [2004] compared 23 CMEs that were preceded (P) by other wide ($\geq$60°) CMEs with the 20 CMEs that were not preceded (NP) by such CMEs. The P and NP CME groups differed little in their average speeds and widths, median masses and kinetic energies, and type II burst associations. However, the median peak SEP intensity of the P group exceeded that of the NP group by a factor of seven. Further, the extent of the scatter in the correlation plots between peak SEP intensity and CME speed [*Kahler*, 2001] was greatly reduced when the P and NP CME groups were plotted separately. *Gopalswamy et al.* [2004] offered three reasons for the considerably enhanced SEP intensities of the P CMEs. First, the preceding CME provides an enhanced particle density which lowers the Alfven speed, allowing stronger shocks and SEP intensities. Second, closed field lines in the preceding CMEs could return particles to the shocks for further acceleration, and third, the preceding CME may provide nonthermal seed particles for shock acceleration.

[7] In this work we examine interactions of fast and wide CMEs with the coronal environment for possible factors in resulting SEP peak intensities. We consider preceding and possibly interacting CMEs, streamer-CME relationships, and CME brightness. In contrast to *Gopalswamy et al.* [2003b, 2004], we use 20 MeV SEP events observed with the Energetic Particles: Acceleration, Composition, and Transport (EPACT) [*von Rosenvinge et al.*, 1995] instrument on the Wind spacecraft, which provides a much larger dynamic range of peak SEP intensities than that of the GOES $\geq$ 10 pfu events, to compare SEP-rich and SEP-poor CMEs. We also limit the CME solar source longitudes to W30° to >W90° (referred to as >WL), and we use the CME-streamer interaction classifications of *Subramanian et al.* [1999].

[8] We note that other authors have argued for alternative SEP injection scenarios based on flares [e.g., *Cane et al.*, 2003]. We cannot rule out these scenarios for some SEP events, but arguments against injections from flares have been made [*Tylka et al.*, 2005], and we assume here that gradual SEP events are the products solely of injections from CME-driven shocks.

2. Data Analysis

2.1. Event Selection

[9] The CMEs observed by the LASCO coronagraph on the Solar and Heliospheric Observatory (SOHO) during 1998–2002 and reported at the Catholic University of America (CUA) CME catalog Web site at http://cdaw.gsfc. nasa.gov/CME_list/ were used for this analysis. We began with all fast (>900 km s^{-1}) and wide (>60°) CMEs centered on the west limb or observed as halos. The criteria follow from the recent results that fast CMEs with widths <60° are rarely associated with either gradual SEP events [*Kahler and Reames*, 2003] or DH type II radio bursts [*Gopalswamy et al.*, 2001a], both of which are products of CME-driven shocks. The CME parameters of the CUA catalog are subject to revision; here we have used values current in August 2004. Solar Hα flare reports and EUV and X-ray image data were used to make solar source associations for as many of the CMEs as possible. We then restricted the candidate CMEs with solar source associations to those in the longitude range W30° to over the west limb (>WL). This eliminated CMEs near central meridian, which are unfavorable for observing preceding cospatial CMEs, and eastern hemisphere CMEs, which are unfavorable for observing associated SEP events.

[10] We added to this list all wide CMEs from the W30° to >WL source region that had associated 20 MeV SEP events, regardless of the CME speeds. As in the study of *Kahler and Reames* [2003], the association of a SEP event with a CME was considered to be indeterminate if no increase in SEP intensity was seen above an ambient level of 10^{-2} p cm^{-2} s^{-1} sr^{-1} MeV^{-1}. When no event was detected above a lower SEP intensity level for ~10 hours following a fast CME, the associated SEP intensity was arbitrarily assigned a value of 3 × 10^{-4} p cm^{-2} s^{-1} sr^{-1} MeV^{-1}, the approximate intensity equivalent of the the background counting rate. This procedure yielded a total of 116 wide CMEs in the W30° to >WL longitude range. The logs of peak 20 MeV proton intensities are plotted against the associated CME speeds in Figure 1. The diagonal line is the least-squares best fit to all the events.

Table 1. SEP-Rich and SEP-Poor CMEs

Date	U.T.	Speed[a]	Source	24,12[b]	Strm.Int.[c]	Width[d]	Mass Dens.[e]	20 MeV[f]
				SEP-RICH				
98 20-Apr	10:07	1863	S43W90	1,1	4 at S30	84°	7.8e + 13	30
98 6-May	08:29	1099	S11W65	1,1	2 at N20	94°	4.6e + 13	4
00 18-Feb	09:54	890	>WL	4,1	2 at N20	97°	6.0e + 13	0.4
00 10-Jun	17:08	1108	N22W38	4,1	2 at N45	*120°*	4.6e + 13	1.3
00 25-Oct	08:26	770	W50	2,1	4 at S45	*127°*	5.1e + 13	0.25
00 8-Nov	23:06	1738	N10W77	3,1	2 at N20	N.A.	N.A.	40
01 28-Jan	15:54	916	S04W59	1,1	4 at S10	122°	9.3e + 13	0.8
01 12-Apr	10:31	1184	S19W43	2,1	2 at S20	*132°*	2.6e + 13	0.9
01 15-Apr	14:06	1199	S20W85	5,2	4 at S20	108°	6.2e + 13	20
01 20-May	06:26	546	>WL	4,0	3 at S30	125°	4.0e + 13	0.15
01 15-Sep	11:54	478	S21W49	1,1	4 at S40	75°	7.9e + 13	0.2
01 1-Oct	05:30	1405	S18W80	1,1	4 at S40	*111°*	1.0e + 14	8.
01 26-Dec	05:30	1446	N08W54	3,2	4 at N15	95°	5.7e + 13	10.
02 22-Aug	02:06	1005	S07W62	2,0	2 at S50	*99°*	7.8e + 13	0.4
02 24-Aug	01:27	1878	S02W81	5,4	2 at S40	*121°*	1.0e + 14	6.
				SEP-POOR				
99 28-Jun	21:30	1083	N26W41	1,1	3 at N60	*40°*	3.1e + 13	<0.0003
99 19-Sep	17:18	1144	N21W71	0,0	3 in NW	N.A.	N.A.	<0.0003
99 21-Sep	03:30	1402	N19W90	1,0	3 in NW	48°	2.4e + 13	<0.0005
99 23-Sep	15:54	1150	W60	0,0	3 at S30	33°	1.1e + 13	<0.0003
99 24-Oct	11:26	1127	>NWL	3,1	2 at N30	63°	1.3e + 13	<.0005
00 4-May	04:50	1064	S14W90	1,1	2 at S30	51°	1.3e + 13	<.0003
00 7-May	20:50	1781	>WL	1,0	2 at S10	*42°*	7.2e + 12	<.002
00 11-Aug	07:31	1071	N27W90	0,0	2 at N00	74°	7.4e + 12	<0.0005
01 20-Mar	08:06	1130	> SWL	2,1	2 at S45	85°	1.2e + 13	<.0003
01 19-Jul	10:30	1668	S08W62	1,0	2 at S20	66°	3.1e + 13	0.0008
02 7-May	00:06	1222	N30W80	2,1	2 at N20	83°	2.7e + 13	<.005
02 10-May	17:06	1154	>NWL	1,1	2 at N20	81°	2.9e + 13	<0.002
02 22-May	00:06	1136	S25W64	1,0	2 at S45	106°	5.9e + 13	<.0005
02 30-May	05:06	1625	>WL	0,0	3 at N00	129°	2.0e + 13	<.0005
02 6-Aug	18:25	1098	S30W30	1,0	2 at S90	71°	9.4e + 13	<.0008
02 22-Dec	03:30	1071	N23W42	0,0	3 at N50	109°	4.7e + 13	<0.001

[a]Units of km s^{-1} from CUA catalog as of August 2004.
[b]Number of preceding CMEs during previous 24 or 12 hours.
[c]CME-streamer interaction type (2, displaced from streamer; 3, no effect; 4, streamer blowout (SB)) and latitude.
[d]Widths determined for CME in the C2 field of view. Italicized widths were halo events in the CUA catalog.
[e]In units of grams/degree.
[f]Peak proton intensity in p cm^{-2} s^{-1} sr^{-1} MeV^{-1}.

[11] We selected for comparison two groups of CMEs from the plot: 15 SEP-rich CMEs lying above the dashed line and 16 SEP-poor CMEs lying below the dashed-dotted line. The point here is to select events that lie farthest from the general correlation between logs of SEP intensity and CME speed, i.e., to remove the CME speed bias from the comparison. All but one of the SEP-poor CMEs showed no apparent SEP enhancements. Many CMEs are clustered together in the range of 900 to 1100 km s^{-1} with no SEP associations; we selected only those with speeds >1060 km s^{-1} for the SEP-poor CME group. The CMEs are listed in Table 1. The first four columns give for each LASCO CME the date and time of first observation, the speed in km s^{-1}, and the source region. The last column gives the peak 20 MeV proton intensity.

[12] We now compare the properties of the two CME groups and ask what environmental effects might be responsible for their extreme differences in SEP production. We note first that the CME accelerations are similar for the two groups. The range and median values for the SEP-rich CMEs are −40 to +98 m s^{-2} and 0 m s^{-2}; those of the SEP-poor CMEs are −90 to +82 m s^{-2} and −6 m s^{-2}. However, only three of the 16 SEP-poor CMEs, but 11 of the 15 SEP-rich CMEs, were associated with possible type II and IV radio bursts in the DH range of the WAVES

experiment on the Wind spacecraft, which are listed at http://lep694. gsfc.nasa.gov/waves/waves.html. This result is expected from the recent comparison of SEP events with DH type II and IV bursts [*Gopalswamy*, 2003; *Gopalswamy et al.*, 2003b; *Cliver et al.*, 2004, Table 1].

2.2. Comparisons of SEP-Rich and SEP-Poor CMEs

2.2.1. Preceding CMEs

[13] Following the work of *Gopalswamy et al.* [2003b, 2004], we examined the cospatial CMEs preceding the primary SEP-rich and SEP-poor CMEs by up to 24 hours. However, we differed from that work by including all preceding CMEs with widths >40° rather than their limit of >60° and by requiring that there be an angular overlap >30° between primary and preceding CMEs rather than using their criterion that the preceding and primary CMEs occur in the same source region. The approach here is to be more inclusive than were *Gopalswamy et al.* [2003b, 2004] in considering interactions between preceding and primary CMEs. We also considered the numbers of preceding CME onsets for the 12 and 24-hour intervals rather than the *Gopalswamy et al.* [2003b, 2004] criterion of only 24-hour periods. We used the CME position angles and widths given in the CUA catalog, but for the eight halo events (six SEP-rich and two SEP-poor, indicated by italics in

Table 2. Distributions of the Numbers of Preceding CMEs for Different Periods

Period	# CMEs	SEP-rich	SEP-poor
Preceding 24 hours	0	0	5
	1	5	8
	2	3	2
	3	2	1
	4	3	0
	5	2	0
	Average	2.6	0.75
Preceding 12 hours	0	2	10
	1	10	6
	2	2	0
	3	0	0
	4	1	0
	Average	1.2	0.4
Preceding 12 hours & <30 R⊙	0	7	14
	1	6	2
	2	2	0
	Average	0.7	0.1

column 7 of Table 1) we redefined the primary CME angular widths to be those observed when the CME was still in the C2 field of view. In several cases this reduced the number of preceding CMEs with required angular overlap. The numbers of preceding CMEs for each primary CME are given in column 5 of Table 1.

[14] Table 2 shows the distributions of the numbers of cases of preceding CMEs for the 15 SEP-rich and 16 SEP-poor CMEs. For both the 12 and 24-hour periods the average number of preceding CMEs was about 3 times larger for the SEP-rich than for the SEP-poor events. In the preceding 12-hour periods, 13 of the 15 SEP-rich CMEs and only six of 16 SEP-poor CMEs were associated with preceding CMEs. On the basis of use of the proton, height-time, and X-ray (PHTX) plots from the CUA catalog, we asked whether the primary CMEs may have overtaken the preceding CMEs using the method of *Gopalswamy et al.* [2002b] of extending to 30 R⊙ the trajectories observed within the LASCO field of view. These results are given in the bottom of Table 2, where we see that only two of 16 SEP-poor CMEs and eight of the 15 SEP-rich CMEs were found possibly to interact with preceding CMEs within 30 R⊙.

2.2.2. CME-Streamer Interactions

[15] We have investigated CME-streamer interactions by adopting the following CME classification scheme of *Subramanian et al.* [1999]: (1) created a streamer; (2) displaced from the streamer; (3) no effect on the streamer; and (4) streamer blowout (SB). CMEs in category 1 result in more coronal material present after the CME than before; we found no CMEs in our analysis fitting that description when comparing coronal images about 4 hours after the CME with images of the pre-CME corona. Whether a particular CME overlapping a coronal feature unchanged by the CME belongs to category 2 or to category 3 depends on whether the coronal feature is considered bright enough to be a streamer. Direct LASCO C2 images and synoptic maps were used to make those judgments using an empirical visual streamer brightness threshold. The SB category includes CMEs for which all or part of the preexisting streamer structure disappears after the CME. Figure 2 shows examples of each of the three categories, and column 6 of Table 1 gives the category of each CME and the approximate observed latitude. The resulting category distributions

are given in Table 3. Large fractions of both groups were found displaced from streamers, but the obvious difference between the two groups lies in the SB and no-effect categories. About half (7/15) of the SEP-rich CMEs were SBs, but the SEP-poor CMEs occurring at streamers had no effect on the streamers.

2.2.3. CME Brightness

[16] We compared the CME brightness of the SEP-rich and SEP-poor CMEs in the 3 to 5 R⊙ height range of the LASCO C2 coronagraph. A visual survey showed that the SEP-rich CMEs were generally brighter than the SEP-poor CMEs. Figure 3 compares two SEP-rich CMEs with two SEP-poor CMEs.

[17] The CME excess brightness or equivalent excess mass can be easily calculated from the calibrated LASCO images. The details of CME mass calculations have been described elsewhere [e.g., *Poland et al.*, 1981; *Vourlidas et al.*, 2000]. In brief, we calculate the mass by subtracting from the frame that contains the CME a suitable preevent image and then summing over all pixels enclosed within the measured width of the CME, from the occulter to the measured front. Usually, the mass is measured at large heights (>10 R⊙) after the CME is well developed and most of the ejected mass has emerged from behind the occulter. In our case, we are interested in the initial stages of the CME development and therefore in the mass of the CME within the LASCO C2 field of view (<6 R⊙). Thus for each CME in our sample, we selected the last C2 image containing the front and measured the mass. To avoid overestimation of the mass, we independently measured the CME widths and took the CME front height and speed from the CUA catalog. We could not find a suitable preevent C2 image for two events (19 September 1999 and 8 November 2000) but were able to calculate statistics for the remaining 29 events. The final CME widths for the mass calculations vary from 33° to 132° and the front heights from 3 to 6.5 R⊙, which means a large variation in CME size within our sample. Therefore we calculated not only the mass but also the mass density in grams per 11.9 arcsec pixel (gr/pix). The angular mass density (CME mass divided by CME angular width in gr/deg) is also a useful parameter when the depth along the line of sight is of interest. The CME widths and angular mass densities are listed in columns 7 and 8 of Table 1.

[18] We compared our CME groups to the overall sample of LASCO CMEs from 1996 to 2003 [*Vourlidas et al.*, 2002b]. The full sample was processed similarly to our SEP CMEs, selecting only the last C2 measurements for the calculations. We then selected only the CMEs with widths from 33° to 132°, leaving a final sample of 3462 CMEs. A scatterplot of the angular mass densities of the overall CME sample as well as the SEP-rich events and the SEP-poor events as a function of height is shown in Figure 4. The solid line is the average mass density per 0.4 R⊙ bin and clearly shows the mass increase as a function of height (or equivalently time) expected as more mass is ejected into the coronagraph field of view from lower heights. It is evident that the SEP-rich events are at the top end of mass densities and do not follow the mass increase behavior, contrary to the SEP-poor events. The median mass statistics of the three populations in our sample are shown in Table 4. The statistics show that compared with the SEP-poor CMEs, the
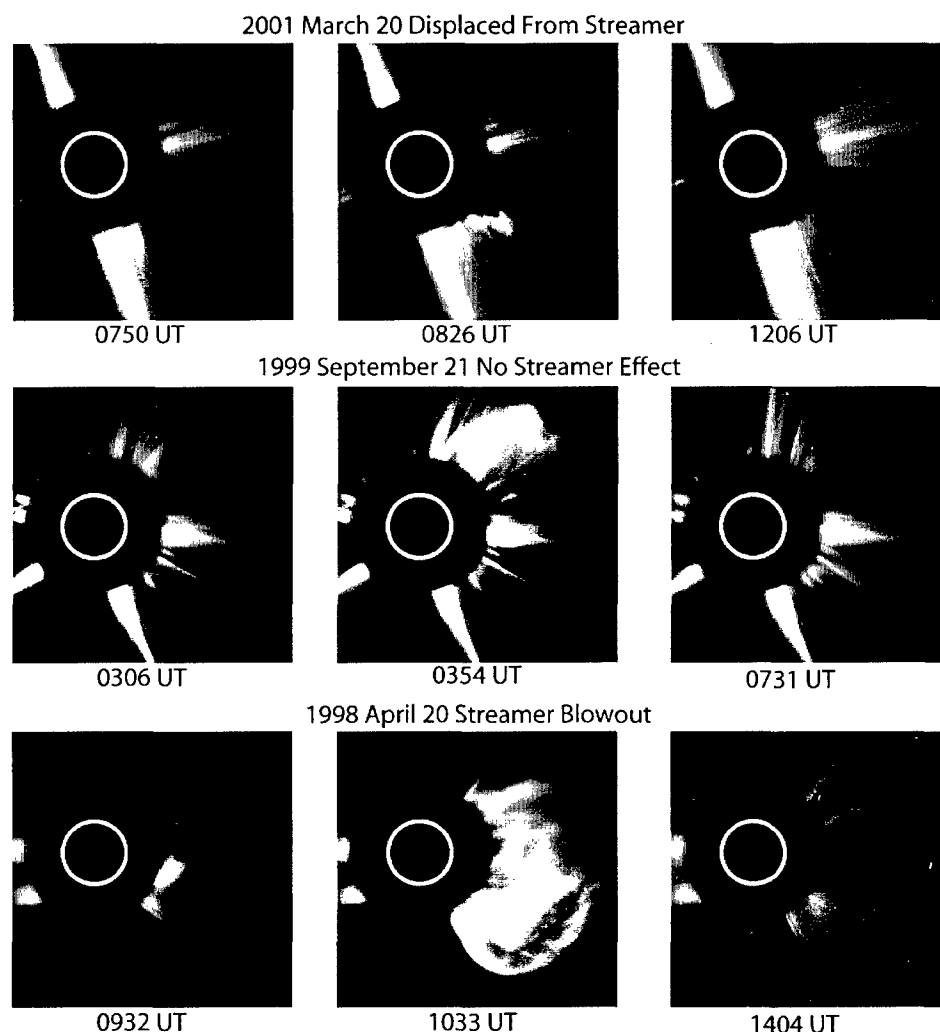
Figure 2. LASCO C2 images of examples of the three categories of CME-streamer interactions. (top) Category 2, displaced from the streamer, on 20 March 2001; (middle) Category 3, no effect on the streamer, on 21 September 1999; (bottom) Category 4, streamer blowout, on 20 April 1998. In each case we show sequences of the pre-CME corona, the CME, and the post-CME corona about 4 hours after the CME onset.

SEP-rich CMEs are more massive and have more mass along the line of sight.

3. Discussion

[19] In this work we have assumed that gradual SEP events are produced solely in CME-driven shocks. We have used LASCO C2 images to compare the coronal environmental characteristics of two groups of fast and wide CMEs, the SEP-rich and SEP-poor CMEs. The two CME groups were separated by at least 3 orders of magnitude in their associated peak 20 MeV proton intensities. We minimized the effects of poor magnetic connection for SEPs and visibility effects for central meridian CMEs by restricting the solar source regions to longitudes of W30° to >WL. An important consideration in such a comparison is to ensure that the properties of the two CME groups are statistically well matched to isolate the factors contributing to SEP production. This applies in particular to the characteristic widths, source longitudes, and speeds of the two CME groups. For our 15 SEP-rich

and 16 SEP-poor CMEs the respective medians are as follows: widths, 109° and 71°; source longitudes, W65° and W85°; and speeds, 1108 and 1140 km s^{-1}. The widths were measured when the CME leading edges were still in the C2 field of view and are significantly larger for the SEP-rich CMEs. We believe that except for the widths the two groups of CMEs are reasonably well matched, which then allows us to focus on the environmental differences that may determine the very disparate peak SEP intensities.

[20] The angular overlap observed between preceding and primary CMEs, similar to the methodology *Gopalswamy et al.* [2002b] was used to search for possible CME interactions. With the same minimum CME speed (900 km s^{-1})

Table 3. CME-Streamer Interactions

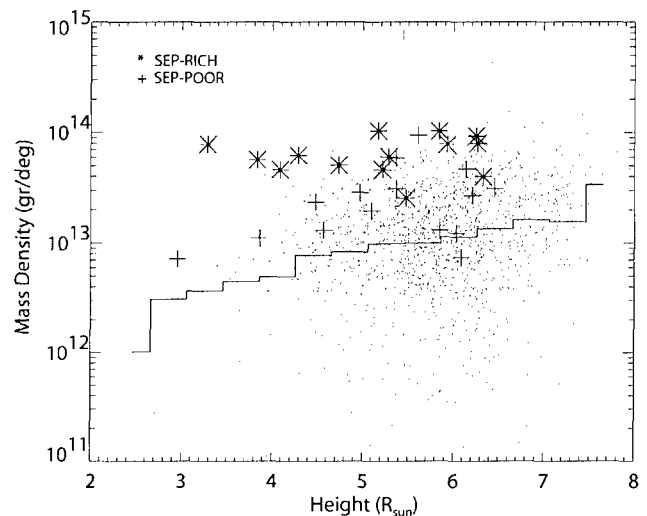| Interaction	SEP-rich	SEP-poor
Displaced from Streamer	7	10
No Effect on Streamer	1	6
Streamer Blowout (SB)	7	0
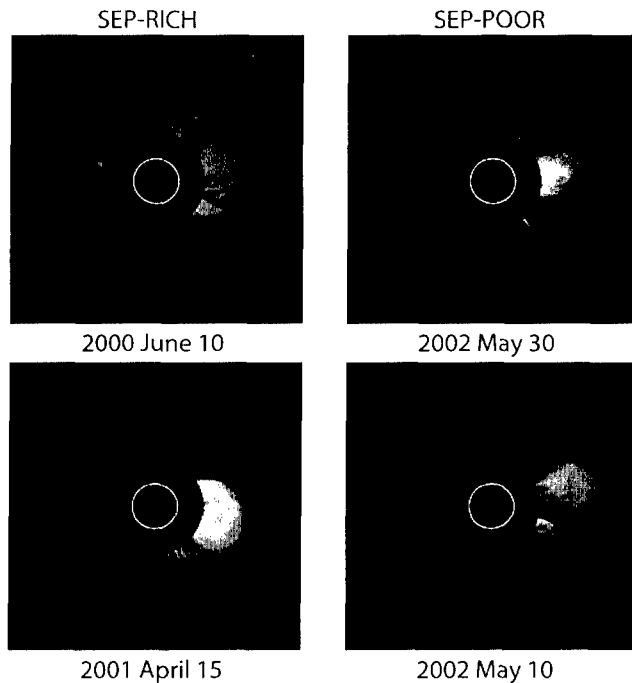
Figure 3. (left) SEP-rich CMEs at 1730 UT on 10 June 2000 (top) and at 1406 UT on 15 April 2001 (bottom). (right) SEP-poor CMEs at 0550 UT on 30 May 2002 (top) and at 1726 UT on 10 May 2002 (bottom). All four LASCO images have been calibrated (excess mass) and scaled identically. The SEP-rich CMEs are clearly larger events in the low corona.

Figure 4. CME mass densities in grams per degree of angular width versus solar height in $R_\odot$. Dots are the 1996–2003 sample of 3462 CMEs with angular widths from 33° to 132°, and the lines show the averages per 0.4 $R_\odot$. Mass densities <1.0e + 11 grams per degree are omitted from the plot. The SEP-rich and SEP-poor events are shown as * and + symbols.

and width (60°) criteria used in our study, they found that SEP-associated CMEs were ~4 times more likely to be preceded by CME interactions than were their SEP-poor CMEs. We also found the same approximate ratio for our SEP-rich and SEP-poor CMEs for 12 or 24 hour periods prior to the primary CMEs. The number of such interactions for CMEs observed in the previous 24 hours was approximately twice that for CMEs observed in the previous 12 hours, suggesting that random chance associations are at work here [*Richardson et al.*, 2003]. We also found no CME interactions occurring within 30 $R_\odot$ for seven of the 15 SEP-rich events. Since the onsets of SEP events usually occur when the primary CMEs are ≲10 $R_\odot$, interactions of the primary CME with the leading edges or even the cores of the preceding CMEs can be ruled out in those cases. Our observational results are therefore consistent with those of *Gopalswamy et al.* [2002b], but we agree with earlier criticism by *Richardson et al.* [2003] and *Kahler* [2003] that CME interactions are not important for SEP production.

[21] The statistics of Table 2 make clear, however, that the rates of overlapping preceding CMEs are much higher for SEP-rich CMEs than for SEP-poor CMEs, consistent with the primary result of *Gopalswamy et al.* [2004]. The preceding CMEs may therefore produce a significant environmental effect on SEP production, perhaps for the reasons offered by *Gopalswamy et al.* [2004].

[22] We compared interactions with coronal streamers for the two CME groups. This approach is limited by the fact that CME measurements and analyses are generally done with differenced coronagraph images that null out the surrounding streamers. Consequently, work on CME-streamer interactions has focused on specific problems such as wave propagation across streamers [*Sheeley et al.*, 2000]. We followed the approach of using the four categories of streamer-CME interactions of *Subramanian et al.* [1999] and tried to apply a consistent standard for streamer interactions to all the CMEs of the study. Our result was that all SEP-poor CMEs were displaced from or had no effect on surrounding streamers, and that was also the case for eight of the 15 SEP-rich CMEs (Table 3). This finding is consistent with the *Subramanian et al.* [1999] result that 73% of their nonhalo CMEs were in the displaced-from-streamer and no-effect-on-streamer categories.

[23] The SB class [*Vourlidas et al.*, 2002a] is the major distinction between SEP-rich CMEs and SEP-poor CMEs. SB CMEs were only 16% of the nonhalo CMEs surveyed by *Subramanian et al.* [1999], but they were nearly half (seven of 15) of the SEP-rich group, so a further comparison of SEP events and SB CMEs may be warranted. The term streamer blowout was introduced by *Howard et al.* [1985] in their classification system of CMEs observed with the Solwind coronagraph; however, it applied to CMEs erupting very slowly (100 to 400 km s⁻¹) following swelling of streamers over periods of many hours. The SB CMEs of this study are very bright and fast (478 to 1863 km s⁻¹) and therefore a very different kind of CME from that considered by *Howard et al.* [1985].

[24] The primary result of this study is that CME brightness, and hence mass, is the most obvious difference

Table 4. CME Mass Distributions

CME Mass	SEP-rich	SEP-poor	All CMEs
Median mass in grams	6.4e + 15	1.2e + 15	6.4e + 14
Median grams/pixel	4.4e + 9	1.8e + 9	6.3e + 8
Median grams/deg	6.2e + 13	2.4e + 13	1.1e + 13

between the SEP-rich and SEP-poor CMEs, as shown in Figure 3. The SEP-rich CMEs lie at the top end of the CME mass-density distribution of Figure 4 and do not follow the general trend of mass increase with height, contrary to the SEP-poor CMEs. The two classes merge at larger heights as more mass enters the LASCO C2 field of view. That is why SEP-rich CMEs cannot be distinguished in the usual statistical mass analyses based on measurements in the outer corona, and it explains why *Gopalswamy et al.* [2004] found similar median masses for their P and NP CMEs. This suggests that further SEP-related CME analysis should be focused on heights $\lesssim 6$ $R_\odot$, where shock acceleration of SEPs is strongest [*Kallenrode*, 1997]. This is well below the ~ 20 $R_\odot$ inner boundary at which some recent shock SEP-acceleration models [e.g., *Rice et al.*, 2003] operate.

[25] The higher mass densities of the SEP-rich CMEs implies that they are either (1) wider along the lines of sight, i.e., in solar longitude, or (2) originate at lower heights in the corona where the density is higher, or (3) both. In the CME-shock paradigm for SEP events we assume that the strength and the spatial extent of the CME-driven collisionless MHD shock are the important factors for the resulting SEP intensity. If we assume a detached shock ahead of the bright CME [*Vourlidas et al.*, 2003], the strength of the CME-driven shock should be governed by the CME speed through the ambient corona and not by the CME mass or density. Thus the result that a high CME brightness is important for SEP production suggests that the SEP-rich CMEs may be unusually broad in longitude. Previous work has established that SEP-associated CMEs must be broad (>60°) in angular width [*Kahler et al.*, 2003; *Gopalswamy et al.*, 2004], which is a measure of latitudinal extent. Our finding that both the SEP-rich CME widths and angular brightness significantly exceed those of the SEP-poor CMEs suggests that the SEP-rich CMEs must be broad in latitude and longitude, perhaps because only a large-angle coronal/interplanetary shock can be effective in producing a sufficient population of SEPs to be detected at 1 AU.

[26] An alternative possibility suggested by the large fraction of SB SEP-rich CMEs (Table 3) is that the SEP-rich CMEs occur in intrinsically dense coronal regions, such as streamers. Their high internal pressures could cause them to expand rapidly in azimuth, driving shocks at their flanks as well as radially. The fact that about half the SEP-rich CMEs had no streamer interactions (Table 3) shows, however, that there is not a required role for streamers in the scenario of SEP acceleration by CME shocks. Finally, we note that CME brightness may be a useful tool for predicting SEP associations with observed CMEs.

References

Cane, H. V., T. T. von Rosenvinge, C. M. S. Cohen, and R. A. Mewaldt (2003), Two components in major solar particle events, *Geophys. Res. Lett.*, *30*(12), 8017, doi:10.1029/2002GL016580.

Cliver, E. W., S. W. Kahler, and D. V. Reames (2004), Coronal shocks and solar energetic proton events, *Astrophys. J.*, *605*, 902.

Gopalswamy, N. (2003), Solar and geospace connections of energetic particle events, *Geophys. Res. Lett.*, *30*(12), 8013, doi:10.1029/2003GL017277.

Gopalswamy, N., S. Yashiro, M. L. Kaiser, R. A. Howard, and J.-L. Bougeret (2001a), Characteristics of coronal mass ejections associated with long-wavelength type II radio bursts, *J. Geophys. Res.*, *106*, 29,219.

Gopalswamy, N., S. Yashiro, M. L. Kaiser, R. A. Howard, and J.-L. Bougeret (2001b), Radio signatures of coronal mass ejection interaction: coronal mass ejection cannibalism?, *Astrophys. J.*, *548*, L91.

Gopalswamy, N., S. Yashiro, M. L. Kaiser, R. A. Howard, and J.-L. Bougeret (2002a), Interplanetary radio emission due to interaction between two coronal mass ejections, *Geophys. Res. Lett.*, *29*(8), 1265, doi:10.1029/2001GL013606.

Gopalswamy, N., S. Yashiro, G. Michalek, M. L. Kaiser, R. A. Howard, D. V. Reames, R. Leske, and T. von Rosenvinge (2002b), Interacting coronal mass ejections and solar energetic particles, *Astrophys. J.*, *572*, L103.

Gopalswamy, N., S. Yashiro, G. Michalek, M. L. Kaiser, R. A. Howard, R. Leske, T. von Rosenvinge, and D. V. Reames (2003a), Effect of CME interactions on the production of solar energetic particles, in *Solar Wind Ten*, edited by M. Velli, R. Bruno, and F. Malara, *AIP Conf. Proc.*, *679*, 608.

Gopalswamy, N., S. Yashiro, A. Lara, M. L. Kaiser, B. J. Thompson, P. T. Gallagher, and R. A. Howard (2003b), Large solar energetic particle events of cycle 23: A global view, *Geophys. Res. Lett.*, *30*(12), 8015, doi:10.1029/2002GL016435.

Gopalswamy, N., S. Yashiro, S. Krucker, G. Stenborg, and R. A. Howard (2004), Intensity variation of large solar energetic particle events associated with coronal mass ejections, *J. Geophys. Res.*, *109*, A12105, doi:10.1029/2004JA010602.

Howard, R. A., N. R. Sheeley Jr., M. J. Koomen, and D. J. Michels (1985), Coronal mass ejections: 1979–1981, *J. Geophys. Res.*, *90*, 8173.

Kahler, S. W. (2001), The correlation between solar energetic particle peak intensities and speeds of coronal mass ejections: Effects of ambient particle intensities and energy spectra, *J. Geophys. Res.*, *106*, 20,947.

Kahler, S. W. (2003), Energetic particle acceleration by coronal mass ejections, *Adv. Space Res.*, *32*(12), 2587.

Kahler, S. W., and D. V. Reames (2003), Solar energetic particle production by coronal mass ejection-driven shocks in solar fast-wind regions, *Astrophys. J.*, *584*, 1063.

Kallenrode, M.-B. (1997), A statistical study of the spatial evolution of shock acceleration efficiency for 5 MeV protons and subsequent particle propagation, *J. Geophys. Res.*, *102*, 22,335.

Poland, A. I., R. A. Howard, M. J. Koomen, D. J. Michels, and N. R. Sheeley Jr. (1981), Coronal transients near sunspot maximum, *Sol. Phys.*, *69*, 169.

Reames, D. V. (1999), Particle acceleration at the Sun and in the heliosphere, *Space Sci. Rev.*, *90*, 413.

Rice, W. K. M., G. P. Zank, and G. Li (2003), Particle acceleration and coronal mass ejection driven shocks: Shocks of arbitrary strength, *J. Geophys. Res.*, *108*(A10), 1369, doi:10.1029/2002JA009756.

Richardson, I. G., G. R. Lawrence, D. K. Haggerty, T. A. Kucera, and A. Szabo (2003), Are CME "interactions" really important for accelerating major solar energetic particle events?, *Geophys. Res. Lett.*, *30*(12), 8014, doi:10.1029/2002GL016424.

Sheeley, N. R., Jr., W. N. Hakala, and Y.-M. Wang (2000), Detection of coronal mass ejection associated shock waves in the outer corona, *J. Geophys. Res.*, *105*, 5081.

Subramanian, P., K. P. Dere, N. B. Rich, and R. A. Howard (1999), The relationship of coronal mass ejections to streamers, *J. Geophys. Res.*, *104*, 22,321.

Tylka, A. J., C. M. S. Cohen, W. F. Dietrich, M. A. Lee, C. G. Maclennan, R. A. Mewaldt, C. K. Ng, and D. V. Reames (2005), Shock geometry, seed populations, and the origin of variable elemental composition at high energies in large gradual solar particle events, *Astrophys. J.*, *625*, 474.

Vandas, M., and D. Odstrcil (2004), Acceleration of electrons by interacting CMEs, *Astron. Astrophys.*, *415*, 755.

von Rosenvinge, T. T., et al. (1995), The Energetic Particles: Acceleration, Composition, and Transport (EPACT) investigation on the Wind spacecraft, *Space Sci. Rev.*, *71*, 155.

Vourlidas, A., P. Subramanian, K. P. Dere, and R. A. Howard (2000), Large-Angle Spectrometric Coronagraph measurements of the energetics of coronal mass ejections, *Astrophys. J.*, *534*, 456.

Vourlidas, A., R. A. Howard, J. S. Morrill, and S. Munz (2002a), Analysis of Lasco observations of streamer blowout events, in *Solar-Terrestrial*

Magnetic Activity and Space Environment, Proc. COSPAR Colloq., vol. 14, edited by H. Wang and R. Xu, p. 201, Elsevier, New York.

Vourlidas, A., D. Buzasi, R. A. Howard, and E. Esfandiari (2002b), Mass and energy properties of LASCO CMEs, in *Proceedings of the 10th European Solar Physics Meeting on Solar Variability: From Core to Outer Frontiers, ESA SP-506*, vol. 1, edited by A. Wilson, p. 91, Eur. Space Agency, Paris.

Vourlidas, A., S. T. Wu, A. H. Wang, P. Subramanian, and R. A. Howard (2003), Direct detection of a coronal mass ejection-associated shock in large angle and spectrometric coronagraph experiment white-light images, *Astrophys. J., 598*, 1392.

S. W. Kahler, Air Force Research Laboratory/VSBXS, 29 Randolph Rd., Hanscom Air Force Base, MA 01731, USA. (stephen.kahler@hanscom.af.mil)

A. Vourlidas, Naval Research Laboratory, Code 7663, 4555 Overlook Avenue SW, Washington, DC 20375, USA. (avourlid@pythia.nrl.navy.mil)